Σ(1385)± resonance production in Pb-Pb collisions at √sNN=5.02 TeV

(ALICE Collaboration) Acharya, S.; ...; Erhardt, Filip; ...; Gotovac, Sven; ...; Jerčić, Marko; ...; Karatović, David; ...; ...

Journal article, Published version
Rad u časopisu, Objavljena verzija rada (izdavačev PDF)

Permanent link / Trajna poveznica: https://urn.nsk.hr/urn:nbn:hr:217:497295

Download date / Datum preuzimanja: **2025-03-07**

THE EUROPEAN
PHYSICAL JOURNAL C

Regular Article - Experimental Physics

$\Sigma(1385)^{\pm}$ resonance production in Pb–Pb collisions at $\sqrt{s_{\mathrm{NN}}} = 5.02$ TeV

ALICE Collaboration[*]

CERN, 1211 Geneva 23, Switzerland

Abstract Hadronic resonances are used to probe the hadron gas produced in the late stage of heavy-ion collisions since they decay on the same timescale, of the order of 1–10 fm/c, as the decoupling time of the system. In the hadron gas, (pseudo)elastic scatterings among the products of resonances that decayed before the kinetic freeze-out and regeneration processes counteract each other, the net effect depending on the resonance lifetime, the duration of the hadronic phase, and the hadronic cross sections at play. In this context, the $\Sigma(1385)^{\pm}$ particle is of particular interest as models predict that regeneration dominates over rescattering despite its relatively short lifetime of about 5.5 fm/c. The first measurement of the $\Sigma(1385)^{\pm}$ resonance production at midrapidity in Pb–Pb collisions at $\sqrt{s_{\mathrm{NN}}} = 5.02$ TeV with the ALICE detector is presented in this Letter. The resonances are reconstructed via their hadronic decay channel, $\Lambda\pi$, as a function of the transverse momentum (p_{T}) and the collision centrality. The results are discussed in comparison with the measured yield of pions and with expectations from the statistical hadronization model as well as commonly employed event generators, including PYTHIA8/Angantyr and EPOS3 coupled to the UrQMD hadronic cascade afterburner. None of the models can describe the data. For $\Sigma(1385)^{\pm}$, a similar behaviour as $K^*(892)^0$ is observed in data unlike the predictions of EPOS3 with afterburner.

1 Introduction

Relativistic heavy–ion (A–A) collisions provide an excellent tool to study nuclear matter under extreme conditions of temperature and density and the phase transition between hadronic matter and a deconfined state of quarks and gluons, the quark–gluon plasma (QGP), predicted by lattice quantum chromodynamics (QCD) calculations [1]. As the QGP produced in a heavy-ion collision expands, it cools down until a phase transition occurs that confines quarks and gluons inside hadrons around a temperature of 155–158 MeV [2]. Soon after hadronisation, the resulting dense and hot gas of stable hadrons and resonances reaches the chemical freeze-out. Afterwards, hadrons keep interacting (pseudo-)elastically, and thus exchanging momentum, until the final decoupling at kinetic freeze-out where their momentum distribution is determined. In this stage, the hadron gas temperature decreases from around 150 MeV to approximately 100 MeV. The late hadronic stage of heavy-ion collisions represents a unique environment for the study of a hadronic system in such conditions of high temperature and density. The understanding of the processes occurring in the excited hadron gas is therefore of primary relevance for the interpretation of observables that are employed to characterize the chemical and kinetic freeze-outs, the hadronic phase and more broadly speaking, the time evolution of a heavy-ion collision. In this respect, short-lived resonances are sensitive probes to study the hadronic phase, which is formed after the chemical freeze-out. This is due to their different lifetimes that are comparable to the expected time duration of the hadronic phase ($\approx$ 1–10 fm/c) [3].

The resonances with the shortest lifetime such as the ρ^0 (lifetime $c\tau \approx 1$ fm [4]) decay during the hadronic phase and their decay products are subject to rescattering effects in the dense hadronic matter, losing memory of the resonance from which they have decayed. Due to the lack of correlation among the decay products, the result is that the resonance cannot be reconstructed via the usual invariant-mass analysis and the measured yield is suppressed with respect to expectations [5]. The resonances with the longest lifetime such as the ϕ ($c\tau \approx 45$ fm [4]) are likely to survive the hadronic phase and decay in vacuum after the kinetic freeze-out. The scenario is further complicated by regeneration effects for which two particles in the hadronic phase interact via resonance formation, producing an enhancement with respect to the primordial production of that resonance. The $\Sigma(1385)^{\pm}$ ($c\tau \approx$ 5.01 fm for $\Sigma(1385)^-$ and $c\tau \approx 5.48$ fm for $\Sigma(1385)^+$ [4]) provides a crucial test case in this context. The typical modeling of the hadronic phase is based on transport codes in which hadronic cross sections are implemented to describe

[*] e-mail: alice-publications@cern.ch

the known hadronic interactions. The widely used hadronic cascade simulator UrQMD [6] is therefore coupled to event generators such as EPOS [7,8] in order to predict the production of hadronic resonances. So far, this picture has been tested mostly with the $K^*(892)^0$ resonance which has a lifetime of $c\tau \approx 4.2$ fm and its production has been measured to be strongly suppressed [9] due to the dominance of rescattering effects. Results from ρ^0 and $\Lambda(1520)$ further support this picture of rescattering [5,10]. Despite its relatively short lifetime, the $\Sigma(1385)^{\pm}$ is expected to be essentially unaffected by the hadronic phase, likely due to larger cross sections for the regeneration processes [11,12]. In this Letter, the first measurement of $\Sigma(1385)^{\pm}$ in heavy-ion collisions at the LHC is reported, based on a data sample of Pb–Pb collisions at a centre-of-mass energy per nucleon pair of $\sqrt{s_{NN}} = 5.02$ TeV. The measurement presented in this Letter provides an essential test of our current understanding of the evolution of hadronisation induced by heavy-ion collisions.

This Letter is organised as follows. After a brief description of the ALICE detector and the data analysis in Sect. 2, the measured transverse-momentum (p_T) spectra and p_T-integrated yields and ratios are presented in Sect. 3 together with a discussion of our findings. Our conclusions are then summarized in Sect. 4.

2 Experiment and data analysis

2.1 Experimental setup and event selection

A detailed description of the ALICE detector and its performance can be found in Refs. [13,14]. This apparatus is optimized for providing particle identification (PID) in a wide momentum range (0.1–20 GeV/c) and high track-density environment by using different techniques. For this analysis, the Inner Tracking System (ITS) and the Time Projection Chamber (TPC) are used for vertex determination and tracking, while the TPC and the Time-Of-Flight (TOF) systems are employed for PID. These detectors cover the full azimuth over a pseudorapidity region $|\eta| < 0.9$ and are located inside a large solenoidal magnet providing a field of 0.5 T. The ITS [15], located at a radial distance $3.9 < r < 43$ cm from the beam axis, consists of two layers of silicon pixels (SPD), two layers of silicon drift chambers and two layers of silicon strips. The SPD, in particular, is used to reconstruct the track segments that serve to determine the primary vertex of the collision. The TPC [16] is a large cylindrical drift chamber covering a radial distance $85 < r < 247$ cm and the main tracking device in the central barrel. The TOF [17] consists of a cylindrical array of MRPCs located at a radial distance of about 380 cm from the beam axis, with an intrinsic resolution of 50 ps. Charged particles can be identified via their specific energy loss, dE/dx, measured in the TPC with

a resolution of 5%, and via their time-of-flight measured by TOF.

On either sides of the interaction point, two scintillator hodoscopes, the V0A ($2.8 < \eta < 5.1$) and V0C ($-3.7 < \eta < -1.7$) [18], serve for triggering, background rejection and centrality classification, as shown in Table 3. In addition, two Zero Degree Calorimeters (ZDC) [19] placed at equal distances, 112.5 m, from the interaction region are used for background rejection and spectator nucleon measurements.

The data samples analysed were recorded in 2018 using Pb–Pb collisions at $\sqrt{s_{NN}} = 5.02$ TeV. The minimum bias (MB) interaction trigger during the data collection requires a coincidence of signals in the V0A and V0C. The central and semi-central triggers require in addition to the MB trigger, an online selection on the total signal amplitude in the V0 detectors, corresponding to collision centralities of 0–10% and 30–50%, respectively. Background events are rejected using the timing information from the ZDC and the V0 detectors [20]. For the pile-up removal, the correlations between the number of reconstructed space points (clusters) in the SPD, the number of reconstructed SPD track segments and the total signal in the V0A and V0C detectors are considered.

Events are selected only if they contain at least two tracks and a reconstructed primary vertex located within ± 10 cm with respect to the nominal interaction point along the beam axis (z axis). A total of 26×10^7 collision events have been accepted for the analysis. Events are further classified into centrality classes, expressed in terms of percentiles of the total hadronic Pb–Pb cross section, using the signal amplitudes in the V0 arrays [20–22]. The analysis is performed in three centrality classes: 0–10%, 30–50% and 50–90%. The 0–10% and 50–90% centrality classes correspond to the most central and the most peripheral Pb–Pb collisions with small and large impact parameters, respectively.

2.2 Resonance reconstruction and yield extraction

The resonances $\Sigma(1385)^+$ and $\Sigma(1385)^-$ are measured separately via their hadronic decay channel to Λ and $\pi^{\pm}$ with a branching ratio of 87% [4], by calculating their invariant mass. The Λ decays weakly into a pπ pair with a branching ratio of 63.9% and a characteristic V^0 topology, which is exploited for its reconstruction. In the following, when referring to $\Sigma(1385)^+$ or $\Sigma(1385)^-$, the sum of the particle and antiparticle (cc, charge conjugate) is considered.

Primary charged tracks are required to fulfill the standard criteria for good reconstruction quality described in Ref. [23]. These selections affect the $\pi^{\pm}$ from the $\Sigma(1385)^{\pm}$ decays, for which it is additionally required to have $p_T > 120$ MeV/c. Pion identification is based on the requirement that the dE/dx and the time-of-flight measured in the TPC and in the TOF, respectively, are compatible with their expected values within

Table 1 Selection criteria of the Λ daughter of $\Sigma(1385)^{\pm}$

$\|y_\Lambda\|$	< 0.5
DCA of the proton daughter to primary vertex	> 0.12 cm
DCA of the pion daughter to primary vertex	> 0.3 cm
DCA between Λ decay products	< 0.8 standard deviations
Λ cosine of pointing angle	> 0.98
Λ invariant mass window	$m_{\mathrm{PDG}} \pm 6.7$ MeV/c^2
Λ decay radius (R_Λ)	$5 < R_\Lambda < 200$ cm
Proper lifetime	< 25 cm/c
Daughters p_{T}	> 150 MeV/c

a fixed number of standard deviations (σ_{TPC}, σ_{TOF}) [24]. In particular, the signals are requested to be within $\pm 5\sigma_{\mathrm{TPC}}$, $\pm 3\sigma_{\mathrm{TPC}}$ and $\pm 2\sigma_{\mathrm{TPC}}$ for tracks with $p_{\mathrm{T}} < 0.35$ GeV/c, $0.35 < p_{\mathrm{T}} < 0.5$ GeV/c, and $0.5 < p_{\mathrm{T}} < 20$ GeV/c, respectively. If the measurement of the time-of-flight is available, this information is used in combination with the TPC PID by applying a selection based on a $\pm 3\sigma_{\mathrm{TOF}}$ range if $p_{\mathrm{T}} < 1.5$ GeV/c and on a $\pm 2.5\sigma_{\mathrm{TOF}}$ range otherwise.

For the decay products (daughters) of the Λ, a subset of the standard track quality criteria are applied with the addition of $p_{\mathrm{T}} > 150$ MeV/c. Furthermore, the candidate Λs fulfill the criteria of the V^0 decay topology listed in Table 1. The distance of closest approach (DCA) of the Λ daughters is measured in standard deviations of this distribution. The pointing angle is the angle between the direction of the momentum of the Λ and the line connecting the secondary to the primary vertex. The invariant mass window is defined so as to take into account the resolution of the reconstructed Λ and R_Λ is the allowed radial distance within which the Λ decay is considered. The Λ daughters are identified as pions and protons based on a $4\sigma_{\mathrm{TPC}}$ criterium for all p_{T}.

The $\Lambda\pi$ pairs are reconstructed within the region $|\eta| < 0.8$ and $|y| < 0.5$ by combining candidates from the same event. The uncorrelated combinatorial background is estimated via the mixed-event technique, by combining Λ and pions belonging to different events of the same centrality class with similar primary vertex position along the z-axis and charged-particle multiplicity. Specifically, the difference among the z-coordinate of the vertices of the events being mixed must be less than 1 cm and the difference of the charged-particle multiplicities less than five. To reduce the statistical fluctuations in the mixed-event background distribution, each event is mixed with nine other events.

As the $\Sigma(1385)^{\pm}$ decay products have a large mass difference, a selection on their momenta is applied which helps to reduce the combinatorial background under the peak. This is achieved by requiring the momentum asymmetry of the

decay products (defined as $(p_\Lambda - p_\pi)/(p_\Lambda + p_\pi)$) to be between 0.3 and 0.95. The asymmetry selection results in the partial removal of the correlated background remaining after the event-mixing background subtraction.

The criteria used to select the $\Lambda\pi$ pairs are applied to both same-event and mixed-event invariant mass distributions, which are then normalized in the region $1.8-2.0$ GeV/c^2. The normalised mixed-event background distributions are subtracted from the same-event ones. The resulting invariant mass ($M_{\Lambda\pi}$) distributions exhibit the signal peak on top of a residual background consisting of correlated $\Lambda\pi$ pairs from other particles or misidentified ones [25]. The residual background has a smooth shape that is described by the following function:

$$f_{\mathrm{BG}} = [M_{\Lambda\pi} - (m_\pi + m_\Lambda)]^n \exp(A + B \times M_{\Lambda\pi} + C \times M_{\Lambda\pi}^2),$$
$$(1)$$

where m_π and m_Λ are the π and Λ mass, respectively, taken from Ref. [4] and A, B, C and n are free parameters.

The mixed-event subtracted invariant mass distribution is fitted with a Breit–Wigner function for the signal and Eq. 1 for the residual background. The width of the resonances is kept fixed at the PDG value of 36 MeV/c^2 for $\Sigma(1385)^+$ and 39 MeV/c^2 for $\Sigma(1385)^-$ [4]. This procedure is repeated in nine intervals in the pair p_{T}, from 1 to 9 GeV/c, and for each centrality class. The fit range for each p_{T} interval varies in order to achieve a better χ^2 per degree of freedom. The lower values vary between 1.26 and 1.30 GeV/c^2 and the upper boundaries from 1.55 to 1.70 GeV/c^2. The yields of $\Sigma(1385)^{\pm}$ are extracted in each p_{T} interval and centrality class by integrating the Breit–Wigner function in the range $[M_{\mathrm{p}} - 5\Gamma, M_{\mathrm{p}} + 5\Gamma]$, where M_{p} is the peak position resulting from the fit and Γ the width of the resonance. In Fig. 1, the mixed-event subtracted invariant mass distribution is presented for $\Sigma(1385)^+$ (left) in the 0–10% centrality class for $3.5 < p_{\mathrm{T}} < 4.5$ GeV/c and for $\Sigma(1385)^-$ (right) in the 30–50% centrality class for $2.5 < p_{\mathrm{T}} < 3.5$ GeV/c. In the latter, the Ξ peak is visible at ≈ 1.321 GeV/c^2, requiring for $\Sigma(1385)^-$ an additional gaussian function to be used in the fit to take into account the Ξ particle.

2.3 Corrections

The extracted raw yields of $\Sigma(1385)^{\pm}$ are normalized to the number of events of the corresponding centrality class and corrected for the detector acceptance (A), the reconstruction efficiency (ϵ_{rec}) and the branching ratio (BR) [4]. The detector acceptance and reconstruction efficiency (called efficiency) are determined from a Monte Carlo simulation based on the HIJING event generator [26]. The $\Sigma(1385)^{\pm}$ signals are injected with a flat p_{T} distribution in the range
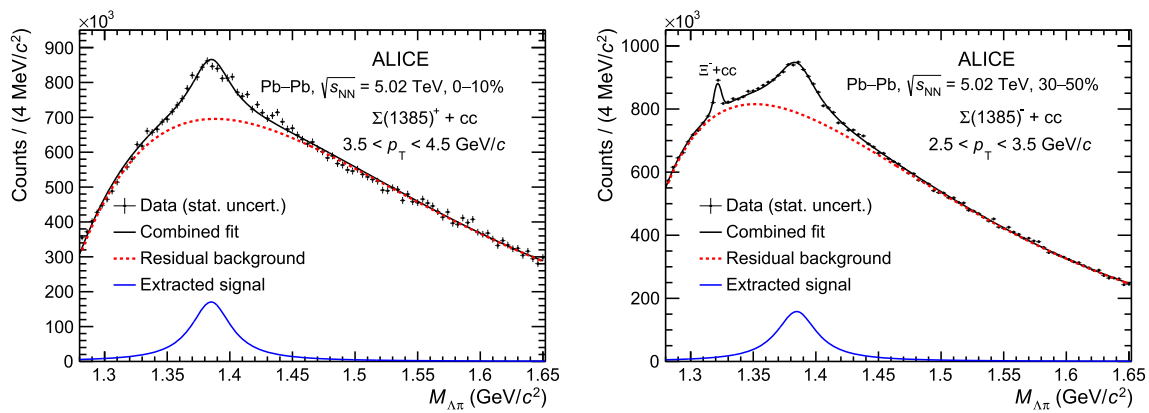
Fig. 1 Left:Invariant mass distribution of $\Lambda\pi$ pairs for $\Sigma(1385)^+$ after subtraction of the mixed-event background in 0–10% central Pb–Pb collisions and $3.5 < p_T < 4.5$ GeV/c. Right:Invariant mass distribution of $\Lambda\pi$ pairs for $\Sigma(1385)^-$ after subtraction of the mixed-event back-ground in 30–50% centrality class and $2.5 < p_T < 3.5$ GeV/c. The black curves represent the combined fit using a signal (continuous blue line) plus residual background (red dashed line) model, as described in the text
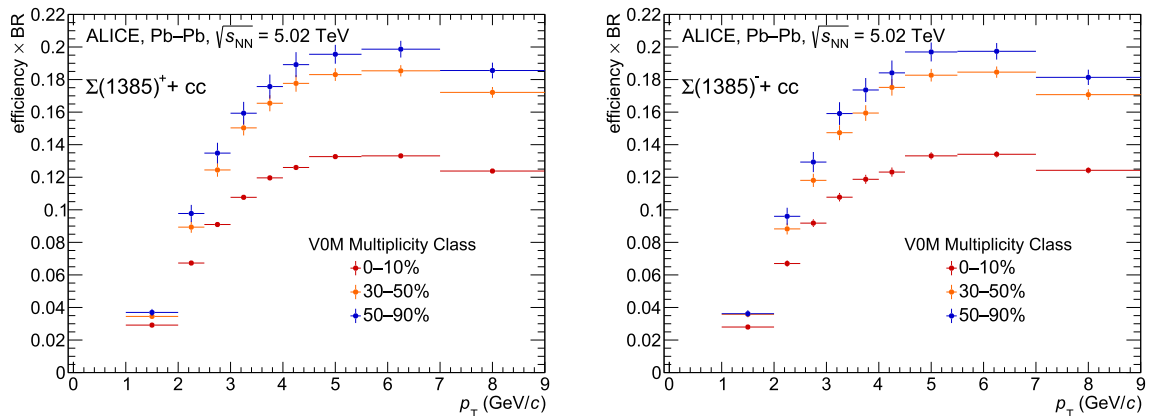
Fig. 2 The product of efficiency×BR for $\Sigma(1385)^+$ (left) and $\Sigma(1385)^-$ (right) in the three centrality classes used for the analysis. The branching ratio, BR, is included in the correction. The error bars represent the statistical uncertainties

$0-10$ GeV/c^2 into HIJING events. The generated particles and their decay products are propagated through the detector material using GEANT3 as transport code [27]. The same criteria are applied to select the resonance decay products and the pairs as for the data analysis. The product $A \times \epsilon_{rec} \times BR$ is calculated as the fraction of the generated $\Sigma(1385)^\pm$ at midrapidity, reconstructed and identified after the application of all selection criteria. The calculation is performed in each centrality class and in Fig. 2, the $A \times \epsilon_{rec} \times BR$ (denoted as efficiency×BR) is shown as a function of p_T for the three centrality classes. It depends on the centrality due to the centrality dependence of the efficiency of both π and Λ particles. Due to the flat input p_T spectrum of the injected $\Sigma(1385)^\pm$ resonances, an iterative procedure is applied for re-weighting it, to remove input spectrum shape effects. The efficiencies obtained from the above described procedure are compared with those obtained from standard HIJING simulations and their ratio is compatible with unity.

2.4 Systematic uncertainties

The sources of systematic uncertainties in the measurement of the $\Sigma(1385)^\pm$ resonances are the yield extraction, the tracking efficiency of the pion daughter, the selection criteria of Λ particles, the pion PID, the knowledge of the detector material budget, the asymmetry selection of the resonance daughter particles and the branching ratio to the decay channel used in the analysis. The uncertainties, except those of the asymmetry and the branching ratio, are p_T and centrality dependent. The uncertainty on the raw yield extraction comprises variations of the fit range, of the background fit function and of the mixed-event background normalization range, the use of bin counting instead of the integration of the signal function, as well as letting the width of the Breit–Wigner free in the fit. From all variations, the maximum deviation from the nominal value is assigned as systematic uncertainty. The difference between the global tracking effi-

Table 2 Sources of systematic uncertainties on the $\Sigma(1385)^{\pm}$ resonance yields in 0–10% most central Pb–Pb collisions at $\sqrt{s_{\mathrm{NN}}}$ = 5.02 TeV, given for two different p_{T} intervals, 1–2 GeV/c and 5.5–7 GeV/c

Systematic variation	$\Sigma(1385)^{+}$ + cc p_{T} (GeV/c)		$\Sigma(1385)^{-}$ + cc p_{T} (GeV/c)	
	1–2	5.5–7	1–2	5.5–7
Yield extraction (%)	13.0	13.2	15.5	13.6
Global tracking efficiency (%)	5.0	3.0	5.0	3.0
Λ topological cuts (%)	3.3	5.1	2.6	4.3
Pion PID (%)	4.1	4.2	2.1	7.7
Material budget (%)	5.2	1.5	5.2	1.5
Daughters asymmetry (%)	5.0	5.0	5.0	5.0
Branching ratio (%)	1.1	1.1	1.1	1.1
Total (%)	16.0	15.8	17.6	17.1
Total multipl. uncorrelated (%)	9.8	5.3	9.7	6.1

ciency in the data and the Monte Carlo simulation contributes to the total uncertainty by affecting the pion daughter and it varies from 5% at $p_{\mathrm{T}} = 1$ GeV/c to 3% at $p_{\mathrm{T}} = 6$ GeV/c. The uncertainty due to the Λ topological selection is calculated by varying the DCA of the Λ daughters to the primary vertex, the DCA of the Λ daughters and the cosine of pointing angle. This uncertainty has a value ranging from 2–3% at the lowest p_{T} to 4–5% at the highest p_{T}. The uncertainty associated with the pion identification is quantified by varying the selections in the TPC and the TOF detectors, and reaches a maximum value of 8% for $\Sigma(1385)^{-}$ in central collisions. The uncertainty on the yields occurring from the implementation of the material budget in the detector simulation was evaluated by increasing and decreasing the material amount within its systematic uncertainty [14], resulting in a variation of $\pm 4.5\%$. Reconstruction in data and Monte Carlo was done in the two extreme cases and the systematic uncertainty has been estimated on the final observables, which are the p_{T} distributions of the resonances. The asymmetry uncertainty is 5%, regardless of p_{T} and centrality, and is evaluated by varying the accepted asymmetry range. Finally, the branching ratio uncertainty is 1.1% [28]. In Table 2, the uncertainties entering the measurement are given for two p_{T} intervals in 0–10% central collisions. The total systematic uncertainty of $\Sigma(1385)^{-}$ is slightly higher than the uncertainty of $\Sigma(1385)^{+}$ mainly due to the fact that in the yield extraction of the former an additional gaussian function has to be taken into account in the fit to parametrise the Ξ peak. In the other centrality classes the uncertainties are lower.

3 Results and discussion

The transverse-momentum distributions of $\Sigma(1385)^{+}$ and $\Sigma(1385)^{-}$ in Pb–Pb collisions are reported in Fig. 3 and compared to the measurements in inelastic pp collisions at

$\sqrt{s} = 7$ TeV [25] and in non-single diffractive (NSD) p–Pb collisions at $\sqrt{s_{\mathrm{NN}}} = 5.02$ TeV [28].

Each of the Pb–Pb distributions in this figure is fitted individually with a Blast-Wave function [29]. The p_{T}-integrated yields and the mean transverse momentum, $\langle p_{\mathrm{T}} \rangle$, are calculated based on the data where the spectra are measured and on the extrapolation of the Blast-Wave function at low p_{T}. The fraction of the integrated yields in the high-p_{T} extrapolation region is negligible, while this fraction for the low-p_{T} one ranges from 28 to 37%, depending on the collision centrality. The statistical and systematic uncertainties of the p_{T}-integrated yields and the mean p_{T} are evaluated by repeating the fit after moving the spectra within their statistical and systematic uncertainties, respectively. The procedure of the fitting and the calculation of the p_{T}-integrated yields and the mean p_{T} described above is repeated with Boltzmann, Fermi–Dirac, m_{T}-exponential and Lévy-Tsallis [30] functions to calculate an additional systematic uncertainty defined as the maximum deviation of these quantities from the ones obtained with the Blast-Wave fit. The dN/dy and $\langle p_{\mathrm{T}} \rangle$ are reported in Tables 3 and 4, respectively, for the three centrality classes of this analysis. As a part of the total systematic uncertainty is correlated across multiplicity, the uncorrelated part of the uncertainties has been calculated by following a similar procedure as the calculation of the total uncertainty. The multiplicity-uncorrelated uncertainties are represented by the third number in Tables 3 and 4. The mean charged-particle multiplicity density for each centrality class, $\langle \mathrm{d}N_{\mathrm{ch}}/\mathrm{d}\eta \rangle$, is also reported in Table 3. Both dN/dy and $\langle p_{\mathrm{T}} \rangle$ increase with $\langle \mathrm{d}N_{\mathrm{ch}}/\mathrm{d}\eta \rangle$ in Pb–Pb collisions.

From pp to central heavy-ion collisions, the spectra become harder with increasing charged-particle multiplicity, following a similar trend as observed for the other measured light-flavour particles and resonances [9,24]. The $\langle p_{\mathrm{T}} \rangle$ increases from about 1.15 GeV/c in pp collisions to about
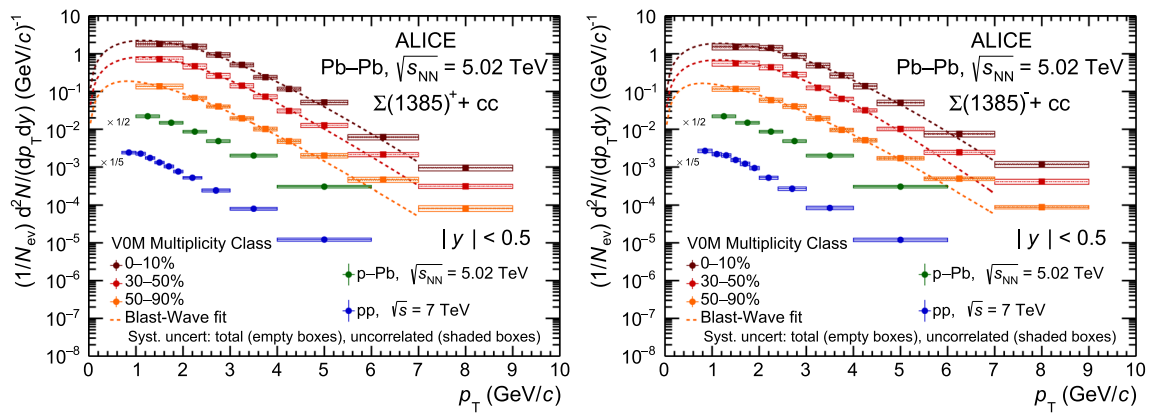
Fig. 3 p_T spectra of $\Sigma(1385)^+$ (left) and $\Sigma(1385)^-$ (right) resonances in Pb–Pb collisions at $\sqrt{s_{NN}}$ = 5.02 TeV in three centrality classes. Empty and shaded boxes depict the total and uncorrelated uncertainties, respectively. The Blast-Wave fit functions are plotted up to 7 GeV/c. The measurements in pp collisions at $\sqrt{s}$ = 7 TeV [25] and in p–Pb collisions at $\sqrt{s}$ = 5.02 TeV (NSD) [28] are quoted for comparisons

Table 3 Average charged-particle multiplicity density per centrality class at midrapidity ($|\eta| < 0.5$) and p_T-integrated yields for $\Sigma(1385)^\pm$. The first, second and third uncertainty in the p_T-integrated yields indicate the statistical, the total systematic uncertainty and the multiplicity-uncorrelated systematic uncertainty, respectively

Class	$\langle dN_{ch}/d\eta \rangle$	dN/dy	
		$\Sigma(1385)^+$ + cc	$\Sigma(1385)^-$ + cc
0–10%	1756.6 ± 51.5	4.956 ± 0.005 ± 0.839 ± 0.550	4.746 ± 0.005 ± 0.871 ± 0.536
30–50%	415.0 ± 13.5	1.851 ± 0.003 ± 0.311 ± 0.158	1.599 ± 0.002 ± 0.266 ± 0.160
50–90%	85.4 ± 9.5	$(3.357 ± 0.007 ± 0.494 ± 0.308) \times 10^{-1}$	$(2.800 ± 0.006 ± 0.471 ± 0.251) \times 10^{-1}$

Table 4 $\langle p_T \rangle$ of $\Sigma(1385)^\pm$ per centrality class. The first, second, and third uncertainty indicate the statistical, the total systematic uncertainty and the multiplicity-uncorrelated systematic uncertainty, respectively

Class	$\langle p_T \rangle$ (GeV/c)	
	$\Sigma(1385)^+$ + cc	$\Sigma(1385)^-$ + cc
0–10%	$(17.185 ± 0.007 ± 0.812 ± 0.748) \times 10^{-1}$	$(16.974 ± 0.007 ± 1.067 ± 0.974) \times 10^{-1}$
30–50%	1.556 ± 0.001 ± 0.068 ± 0.057	1.587 ± 0.001 ± 0.082 ± 0.075
50–90%	1.465 ± 0.001 ± 0.086 ± 0.079	1.551 ± 0.002 ± 0.103 ± 0.070

1.37 GeV/c in p–Pb and further increases with centrality in Pb–Pb as reported in Table 4.

Figure 4 presents the ratios of the measured spectra of the summed $\Sigma(1385)^\pm$ resonance states to the distributions obtained from the EPOS3 and PYTHIA8/Angantyr Monte Carlo event generators in the three Pb–Pb centrality classes.

The EPOS3 model [7,8,31] describes the evolution of a heavy-ion collision with the reaction volume being divided into a core and a corona part. For high string densities, the model does not allow the strings to decay independently, instead, if the energy density from string segments is high enough, these fuse into the so-called "core" region, which evolves hydrodynamically. The low energy density region forms the "corona", which hadronizes according to the unmodified string fragmentation. After hadronization,

hadrons are fed into the UrQMD hadron cascade afterburner, which describes hadronic interactions in a microscopic approach [6]. Previous ALICE measurements of $\rho(770)^0$, $K^*(892)^0$ and $\Lambda(1520)$ in Pb–Pb collisions at $\sqrt{s_{NN}}$ = 2.76 TeV were compared with predictions from the EPOS 3.107 event generator [5,10,11], indicating that the UrQMD afterburner is necessary for the model to describe the spectral shape of these resonances in central collisions, especially at low p_T. Remarkably, the model calculation with UrQMD in [11] predicted that regeneration effects could balance rescattering in the hadronic phase for the $\Sigma(1385)^\pm$ decay products, resulting in no suppression for this resonance as a function of centrality. The new $\Sigma(1385)^\pm$ data reported in this Letter are compared with the latest version of EPOS3 (EPOS 3.4) both with and without coupling it to the UrQMD
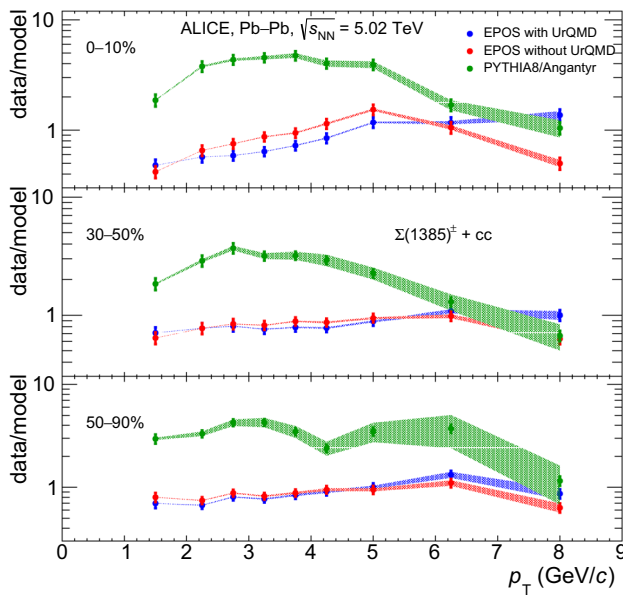
Fig. 4 Ratio of the measured p_T distributions of summed $\Sigma(1385)^\pm$ to model predictions from PYTHIA8/Angantyr (green) and EPOS with (blue) and without (red) the UrQMD afterburner. Each panel corresponds to one of the three centrality classes in Pb–Pb collisions at $\sqrt{s_{NN}} = 5.02$ TeV. Shaded bands represent the model statistical uncertainty, while bars correspond to the data total uncertainties

Fig. 5 $\Sigma(1385)^\pm$ to pion yield ratio measured in ALICE [25,28] together with the STAR measurements [34,35] in various collision systems and energies are reported as a function of the charged-particle multiplicity density at midrapidity, $\langle dN_{ch}/d\eta_{lab}\rangle_{|\eta_{lab}|<0.5}$. Data are compared with model calculations for LHC energies from the GSI–Heidelberg grand canonical statistical hadronization model [2], PYTHIA 8.2 [33], PYTHIA8/Angantyr [32] and EPOS3 with and without UrQMD [31]

afterburner in Fig. 4. No significant difference is observed between the calculation with the UrQMD afterburner and without it in semicentral and peripheral Pb–Pb collisions at $\sqrt{s_{NN}} = 5.02$ TeV. A difference in the two predictions is observed for most central collisions for $1 < p_T < 5$ GeV/c. The model largely overestimates the production of $\Sigma(1385)^\pm$ resonances for $p_T < 5$ GeV/c in 0–10% central Pb–Pb collisions, $\approx 60\%$ in the lowest p_T interval, whereas it describes the data within 20–30% in semicentral and peripheral collisions.

PYTHIA8/Angantyr [32] is an extension of the PYTHIA 8 [33] event generator to the case of heavy-ion collisions. PYTHIA describes nucleon–nucleon interaction at the parton level, based on multiple partonic interactions and Lund-string hadronization. In Angantyr, PYTHIA is extended to model nucleon–nucleus and nucleus–nucleus collisions in a three steps procedure. First, the number of participating nucleons in a collision is calculated from a Glauber-like model. Second, PYTHIA is used to simulate the collision at the partonic level according to the results of the Glauber calculation as a sum of incoherent inelastic, diffractive and/or elastic collisions. Third, the partonic state is allowed to have final state interactions before it is hadronized according to the Lund-string model in PYTHIA. Hadronic rescattering and regeneration processes like those implemented in UrQMD are not considered in the version of PYTHIA8/Angantyr employed here. The data-to-model ratios reported in Fig. 4 show that PYTHIA8/Angantyr underpredicts the $\Sigma(1385)^\pm$ produc-

tion at low momenta by a factor of 3–4 and exhibits a softer spectrum. It only tends to describe the data reasonably well at momenta above $p_T \simeq 7$ GeV/c.

The p_T-integrated yield ratios of $\Sigma(1385)^\pm$ to pions are shown in Fig. 5 for different collision systems as measured by the ALICE [25,28] and the STAR collaborations [34,35]. In general, no particular trend with multiplicity is observed given the uncertainties. A fit with a zeroth order polynomial of all data points reported in Fig. 5 yields a χ^2/NDF of 20.2/10, whereas the exclusion of the Pb–Pb most central point from the fit leads to a χ^2/NDF of 14.6/9. In addition, for the ratio of the most central Pb–Pb point to the pp one, we obtain 0.86 ± 0.16 by taking into account both the statistical and systematic uncertainties, with the latter having the largest contribution to the error of this ratio.

In the same figure, models applicable to different charged-particle multiplicities are also presented. The comparison to the models, concerning especially the higher multiplicities, can give insight to the dominating mechanism in the hadronic phase that results in the observed behaviour. The statistical hadronization model [2] (indicated as GSI-Heidelberg in Fig. 5) describes the process of hadron formation at the scale where perturbative QCD is no longer applicable. It is assumed that near hadronization the fireball created in heavy-ion collisions is close to thermal equilibrium and hadron yields can be characterized by a grand canonical partition function. The prediction compared to data in Fig. 5

is obtained for a chemical freeze-out temperature of T=156 MeV, which results from a fit to the light-flavour hadron and nucleus yields measured by ALICE at the LHC [2]. For the $\rho(770)^0$ [5], $K^*(892)^0$ [9] and $\Lambda(1520)$ [10] short-lived resonances, a suppression with respect to the grand canonical statistical hadronization model expectation is observed for central Pb–Pb collisions, while the data in peripheral collisions are well described. This behaviour, which is also observed for $\Sigma(1385)^\pm$ in Fig. 5, is typically attributed to rescattering in the hadronic phase. In 0–10% central Pb–Pb collisions, the $\Sigma(1385)^\pm$ to pion ratio is 3.6σ lower than the statistical hadronization model prediction, whereas the difference of the zeroth order polynomial fit (without taking into account the most central event class) from the same model is a 3.3σ effect. The calculations from EPOS3 with UrQMD, which is able to describe qualitatively the suppression of the $K^*(892)^0/K$ and $\Lambda(1520)/\Lambda$ yield ratios from central to peripheral Pb–Pb collisions [5,9,10], reproduce qualitatively also the weak centrality dependence of the $\Sigma(1385)^\pm/\pi$ yield ratio. Its magnitude, however, is overpredicted for all centralities.

It is to be noted that the p_T-integrated $\Sigma(1385)^\pm/\pi$ yield ratio (see Fig. 5) in the model exhibits a discrepancy with respect to data that is consistent with the one observed for the $\Sigma(1385)^\pm$ spectrum alone. In both cases, EPOS3 with UrQMD overestimates the production.

The centrality dependence of the $\Sigma(1385)^\pm/\pi$ ratio is qualitatively captured also by PYTHIA8/Angantyr, within the current uncertainties. As PYTHIA8/Angantyr underpredicts the production at low transverse momenta of both $\Sigma(1385)^\pm$ and pions, it consequently underpredicts the p_T-integrated production. Interestingly, this discrepancy is already present in pp collisions [25], indicating that it is not related to the heavy-ion modeling part. The semicentral Pb–Pb point is closer to PYTHIA8/Angantyr prediction because the pion yield is underestimated to a greater degree than the sigma yield.

4 Conclusions

We have presented the first measurement of $\Sigma(1385)^\pm$ production in heavy-ion collisions at LHC energies. An evidence of suppression with respect to the grand canonical thermal model is observed in central collisions as for the $K^*(892)^0$ meson, which has a similar lifetime. While the EPOS3 model coupled to the UrQMD afterburner describes the centrality dependence of the $K^*(892)^0$ data, it clearly overestimates the production of $\Sigma(1385)^\pm$. This may either be caused by a missing element in the model that is common to all centralities or due to the fact that the rescattering and (the seemingly dominant) regeneration effects that EPOS3 withUrQMD predicts for $\Sigma(1385)^\pm$ do not manifest themselves in the data. The current implementation of PYTHIA8/Angantyr does not

reproduce the $\Sigma(1385)^\pm$ yield either, while capturing the centrality dependence of $\Sigma(1385)^\pm/\pi$ within the uncertainties. It remains to be seen if ongoing developments of the model to include hadron rescattering will provide a better agreement with the data.

On the experimental side, future higher precision measurements will clarify if a suppression with respect to pp or peripheral Pb–Pb collisions is present and thus will allow for a model-independent investigation of the rescattering and regeneration picture. In addition, detailed comparisons with future Λ measurements will elucidate if the observed data-model discrepancies are driven by the strangeness content of the hadron under study or the modeling of the hadronic phase.

Data availability statement This manuscript has associated data in a data repository. [Authors' comment: Manuscript has associated data in a HEPData repository at https://www.hepdata.net/record/ins2088201.]

References

1. HotQCD Collaboration, A. Bazazov et al., Equation of state in (2 + 1)-flavor QCD. Phys. Rev. D **90**, 094503 (2014). https://doi.org/10.1103/PhysRevD.90.094503. arXiv:1407.6387 [hep-lat]

2. A. Andronic, P. Braun-Munzinger, K. Redlich, J. Stachel, Decoding the phase structure of QCD via particle production at high energy. Nature **561**, 321–330 (2018). https://doi.org/10.1038/s41586-018-0491-6. arXiv:1710.09425 [nucl-th]

3. ALICE Collaboration, K. Aamodt et al., Two-pion Bose-Einstein correlations in central Pb–Pb collisions at $\sqrt{s_{NN}}$ = 2.76 TeV. Phys. Lett. B **696**, 328–337 (2011). https://doi.org/10.1016/j.physletb.2010.12.053. arXiv:1012.4035 [nucl-ex]

4. Particle Data Group Collaboration, P. Zyla et al., Review of particle physics. PTEP **2020**, 083C01 (2020). https://doi.org/10.1093/ptep/ptaa104

5. ALICE Collaboration, S. Acharya et al., Production of the $\rho(770)^0$ meson in pp and Pb-Pb collisions at $\sqrt{s_{NN}}$ = 2.76 TeV. Phys. Rev. C **99**, 064901 (2019). https://doi.org/10.1103/PhysRevC.99.064901. arXiv:1805.04365 [nucl-ex]

6. M. Bleicher, E. Zabrodin, C. Spieles, S. Bass, C. Ernst et al., Relativistic hadron hadron collisions in the ultrarelativistic quantum molecular dynamics model. J. Phys. G **25**, 1859–1896 (1999). https://doi.org/10.1088/0954-3899/25/9/308. arXiv:hep-ph/9909407

7. H.J. Drescher, M. Hladik, S. Ostapchenko, T. Pierog, K. Werner, Parton based Gribov–Regge theory. Phys. Rep. **350**, 93–289 (2001). https://doi.org/10.1016/S0370-1573(00)00122-8. arXiv:hep-ph/0007198

8. K. Werner, I. Karpenko, T. Pierog, M. Bleicher, K. Mikhailov, Event-by-event simulation of the three-dimensional hydrodynamic evolution from flux tube initial conditions in ultrarelativistic heavy ion collisions. Phys. Rev. C **82**, 044904 (2010). https://doi.org/10.1103/PhysRevC.82.044904. arXiv:1004.0805 [nucl-th]

9. ALICE Collaboration, S. Acharya et al., Evidence of rescattering effect in Pb–Pb collisions at the LHC through production of K*(892)^0 and ϕ(1020) mesons. Phys. Lett. B **802**, 135225 (2020). https://doi.org/10.1016/j.physletb.2020.135225. arXiv:1910.14419 [nucl-ex]

10. ALICE Collaboration, S. Acharya et al., Suppression of Λ(1520) resonance production in central Pb-Pb collisions at $\sqrt{s_{NN}}$ = 2.76 TeV. Phys. Rev. C **99**, 024905 (2019). https://doi.org/10.1103/PhysRevC.99.024905. arXiv:1805.04361 [nucl-ex]

11. A. Knospe, C. Markert, K. Werner, J. Steinheimer, M. Bleicher, Hadronic resonance production and interaction in partonic and hadronic matter in EPOS3 with and without the hadronic afterburner UrQMD. Phys. Rev. C **93**, 014911 (2016). https://doi.org/10.1103/PhysRevC.93.014911. arXiv:1509.07895 [nucl-th]

12. D. Oliinychenko, C. Shen, Resonance production in PbPb collisions at 5.02 TeV via hydrodynamics and hadronic afterburner. arXiv:2105.07539 [hep-ph]

13. ALICE Collaboration, K. Aamodt et al., The ALICE experiment at the CERN LHC. JINST **3**, S08002 (2008). https://doi.org/10.1088/1748-0221/3/08/S08002

14. ALICE Collaboration, B. Abelev et al., Performance of the ALICE Experiment at the CERN LHC. Int. J. Mod. Phys. A **29**, 1430044 (2014). https://doi.org/10.1142/S0217751X14300440. arXiv:1402.4476 [nucl-ex]

15. ALICE Collaboration, K. Aamodt et al., Alignment of the ALICE Inner Tracking System with cosmic-ray tracks. JINST **5**, P03003 (2010)., https://doi.org/10.1088/1748-0221/5/03/P03003. arXiv:1001.0502 [physics.ins-det]

16. J. Alme et al., The ALICE TPC, a large 3-dimensional tracking device with fast readout for ultra-high multiplicity events. Nucl. Instrum. Methods A **622**, 316–367 (2010). arXiv:1001.1950 [physics.ins-det]

17. A. Akindinov et al., Performance of the ALICE time-of-flight detector at the LHC. Eur. Phys. J. Plus **128**, 44 (2013). https://doi.org/10.1140/epjp/i2013-13044-x

18. ALICE Collaboration, E. Abbas et al., Performance of the ALICE VZERO system. JINST **8**, P10016 (2013). https://doi.org/10.1088/1748-0221/8/10/P10016. arXiv:1306.3130 [nucl-ex]

19. R. Arnaldi et al., The zero degree calorimeters for the ALICE experiment. Nucl. Instrum. Methods A **604**, 765 (2009). https://doi.org/10.1016/j.nima.2008.04.009

20. ALICE Collaboration, B. Abelev et al., Centrality determination of Pb-Pb collisions at $\sqrt{s_{NN}}$ = 2.76 TeV with ALICE. *Phys. Rev. C* **88**, 044909 (2013). https://doi.org/10.1103/PhysRevC.88.044909. arXiv:1301.4361 [nucl-ex]
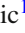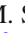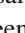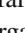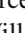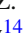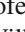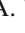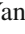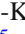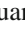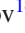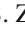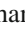
21. ALICE Collaboration, J. Adam et al., Centrality dependence of the charged-particle multiplicity density at midrapidity in Pb–Pb collisions at $\sqrt{s_{NN}}$ = 5.02 TeV. Phys. Rev. Lett. **116**, 222302 (2016). https://doi.org/10.1103/PhysRevLett.116.222302. arXiv:1512.06104 [nucl-ex]

22. ALICE Collaboration, S. Acharya et al., Centrality determination in heavy ion collisions. ALICE-PUBLIC-2018-011. https://cds.cern.ch/record/2636623. Accessed 12 Oct 2020

23. ALICE Collaboration, S. Acharya et al., Non-linear flow modes of identified particles in Pb–Pb collisions at $\sqrt{s_{NN}}$ = 5.02 TeV. JHEP **06**, 147, (2020). https://doi.org/10.1007/JHEP06(2020)147. arXiv:1912.00740 [nucl-ex]

24. ALICE Collaboration, S. Acharya et al., Production of charged pions, kaons, and (anti-)protons in Pb–Pb and inelastic pp collisions at $\sqrt{s_{NN}}$ = 5.02 TeV. Phys. Rev. C **101**, 044907 (2020). https://doi.org/10.1103/PhysRevC.101.044907. arXiv:1910.07678 [nucl-ex]

25. ALICE Collaboration, B. Abelev et al., Production of $\Sigma(1385)^{\pm}$ and $\Xi(1530)^{0}$ in proton–proton collisions at $\sqrt{s}$ = 7 TeV. Eur. Phys. J. C **75**, 1 (2015). https://doi.org/10.1140/epjc/s10052-014-3191-x. arXiv:1406.3206 [nucl-ex]

26. X.-N. Wang, M. Gyulassy, HIJING: a Monte Carlo model for multiple jet production in pp, p–A and A–A collisions. Phys. Rev. D **44**, 3501–3516 (1991). https://doi.org/10.1103/PhysRevD.44.3501

27. R. Brun, F. Bruyant, F. Carminati, S. Giani, M. Maire, A. McPherson, G. Patrick, L. Urban, GEANT detector description and simulation tool. CERN report W5013 (1994), pp. 1–430. https://doi.org/10.17181/CERN.MUHF.DMJ1

28. ALICE Collaboration, D. Adamova et al., Production of $\Sigma(1385)^{\pm}$ and $\Xi(1530)^{0}$ in p–Pb collisions at $\sqrt{s_{NN}}$ = 5.02 TeV.

29. E. Schnedermann, J. Sollfrank, U.W. Heinz, Thermal phenomenology of hadrons from 200-A/GeV S + S collisions. Phys. Rev. C **48**, 2462–2475 (1993). https://doi.org/10.1103/PhysRevC.48.2462. arXiv:9307020 [nucl-th]

30. C. Tsallis, Possible generalization of Boltzmann–Gibbs statistics. J. Stat. Phys. **52**, 479–487 (1988). https://doi.org/10.1007/BF01016429

31. K. Werner, B. Guiot, I. Karpenko, T. Pierog, Analysing radial flow features in p–Pb and p–p collisions at several TeV by studying identified particle production in EPOS3. Phys. Rev. C **89**, 064903 (2014). https://doi.org/10.1103/PhysRevC.89.064903. arXiv:1312.1233 [nucl-th]

32. C. Bierlich, G. Gustafson, L. Lönnblad, H. Shah, The Angantyr model for heavy-ion collisions in PYTHIA8. JHEP **10**, 134 (2018). https://doi.org/10.1007/JHEP10(2018)134. arXiv:1806.10820 [hep-ph]

33. T. Sjöstrand, S. Ask, J.R. Christiansen, R. Corke, N. Desai, P. Ilten, S. Mrenna, S. Prestel, C.O. Rasmussen, P.Z. Skands, An introduction to PYTHIA 8.2. Comput. Phys. Commun. **191**, 159–177 (2015). https://doi.org/10.1016/j.cpc.2015.01.024 arXiv:1410.3012 [hep-ph]

34. STAR Collaboration, J. Adams et al., Strange Baryon Resonance Production in $\sqrt{s_{NN}}$ = 200 GeV p + p and Au + Au Collisions. Phys. Rev. Lett. **97**, 132301 (2006). arXiv:nucl-ex/0604019

35. STAR Collaboration, J. Adams et al., Hadronic resonance production in d+Au collisions at $\sqrt{s_{NN}}$ = 200 GeV measured at the BNL Relativistic Heavy Ion Collider. Phys. Rev. C **78**, 044906 (2008). arXiv:0801.0450 [nucl-ex]

Eur. Phys. J. C **77**, 389 (2017). https://doi.org/10.1140/epjc/s10052-017-4943-1. arXiv:1701.07797 [nucl-ex]

ALICE Collaboration

S. Acharya[125,132], D. Adamová[86], A. Adler[69], G. Aglieri Rinella[32], M. Agnello[29], N. Agrawal[50], Z. Ahammed[132], S. Ahmad[15], S. U. Ahn[70], I. Ahuja[37], A. Akindinov[140], M. Al-Turany[98], D. Aleksandrov[140], B. Alessandro[55], H. M. Alfanda[6], R. Alfaro Molina[66], B. Ali[15], Y. Ali[13], A. Alici[25], N. Alizadehvandchali[114], A. Alkin[32], J. Alme[20], G. Alocco[51], T. Alt[63], I. Altsybeev[140], M. N. Anaam[6], C. Andrei[45], A. Andronic[135], V. Anguelov[95], F. Antinori[53], P. Antonioli[50], C. Anuj[15], N. Apadula[74], L. Aphecetche[104], H. Appelshäuser[63], C. Arata[73], S. Arcelli[25], R. Arnaldi[55], I. C. Arsene[19], M. Arslandok[137], A. Augustinus[32], R. Averbeck[98], S. Aziz[72], M. D. Azmi[15], A. Badalà[52], Y. W. Baek[40], X. Bai[118], R. Bailhache[63], Y. Bailung[47], R. Bala[91], A. Balbino[29], A. Baldisseri[128], B. Balis[2], D. Banerjee[4], Z. Banoo[91], R. Barbera[26], L. Barioglio[96], M. Barlou[78], G. G. Barnaföldi[136], L. S. Barnby[85], V. Barret[125], L. Barreto[110], C. Bartels[117], K. Barth[32], E. Bartsch[63], F. Baruffaldi[27], N. Bastid[125], S. Basu[75], G. Batigne[104], D. Battistini[96], B. Batyunya[141], D. Bauri[46], J. L. Bazo Alba[102], I. G. Bearden[83], C. Beattie[137], P. Becht[98], D. Behera[47], I. Belikov[127], A. D. C. Bell Hechavarria[135], F. Bellini[25], R. Bellwied[114], S. Belokurova[140], V. Belyaev[140], G. Bencedi[136,64], S. Beole[24], A. Bercuci[45], Y. Berdnikov[140], A. Berdnikova[95], L. Bergmann[95], M. G. Besoiu[62], L. Betev[32], P. P. Bhaduri[132], A. Bhasin[91], M. A. Bhat[4], B. Bhattacharjee[41], L. Bianchi[24], N. Bianchi[48], J. Bielčík[35], J. Bielčíková[86], J. Biernat[107], A. P. Bigot[127], A. Bilandzic[96], G. Biro[136], S. Biswas[4], N. Bize[104], J. T. Blair[108], D. Blau[140], M. B. Blidaru[98], N. Bluhme[38], C. Blume[63], G. Boca[21,54], F. Bock[87], T. Bodova[20], A. Bogdanov[140], S. Boi[22], J. Bok[57], L. Boldizsár[136], A. Bolozdynya[140], M. Bombara[37], P. M. Bond[32], G. Bonomi[131,54], H. Borel[128], A. Borissov[140], H. Bossi[137], E. Botta[24], L. Bratrud[63], P. Braun-Munzinger[98], M. Bregant[110], M. Broz[35], G. E. Bruno[97,31], M. D. Buckland[117], D. Budnikov[140], H. Buesching[63], S. Bufalino[29], O. Bugnon[104], P. Buhler[103], Z. Buthelezi[67,121], J. B. Butt[13], A. Bylinkin[116], S. A. Bysiak[107], M. Cai[27,6], H. Caines[137], A. Caliva[98], E. Calvo Villar[102], J. M. M. Camacho[109], P. Camerini[23], F. D. M. Canedo[110], M. Carabas[124], F. Carnesecchi[32], R. Caron[126], J. Castillo Castellanos[128], F. Catalano[29], C. Ceballos Sanchez[141], I. Chakaberia[74], P. Chakraborty[46], S. Chandra[132], S. Chapeland[32], M. Chartier[117], S. Chattopadhyay[132],

S. Chattopadhyay[100], T. G. Chavez[44], T. Cheng[6], C. Cheshkov[126], B. Cheynis[126], V. Chibante Barroso[32],
D. D. Chinellato[111], E. S. Chizzali[96], J. Cho[57], S. Cho[57], P. Chochula[32], P. Christakoglou[84],
C. H. Christensen[83], P. Christiansen[75], T. Chujo[123], M. Ciacco[29], C. Cicalo[51], L. Cifarelli[25], F. Cindolo[50],
M. R. Ciupek[98], G. Clai[50,a], F. Colamaria[49], J. S. Colburn[101], D. Colella[97,31], A. Collu[74], M. Colocci[32],
M. Concas[55,b], G. Conesa Balbastre[73], Z. Conesa del Valle[72], G. Contin[23], J. G. Contreras[35], M. L. Coquet[128],
T. M. Cormier[87,*], P. Cortese[130,55], M. R. Cosentino[112], F. Costa[32], S. Costanza[21,54], P. Crochet[125],
R. Cruz-Torres[74], E. Cuautle[64], P. Cui[6], L. Cunqueiro[87], A. Dainese[53], M. C. Danisch[95], A. Danu[62],
P. Das[80], P. Das[4], S. Das[4], A. R. Dash[135], S. Dash[46], A. De Caro[28], G. de Cataldo[49], L. De Cilladi[24],
J. de Cuveland[38], A. De Falco[22], D. De Gruttola[28], N. De Marco[55], C. De Martin[23], S. De Pasquale[28],
S. Deb[47], H. F. Degenhardt[110], K. R. Deja[133], R. Del Grande[96], L. Dello Stritto[28], W. Deng[6], P. Dhankher[18],
D. Di Bari[31], A. Di Mauro[32], R. A. Diaz[141,7], T. Dietel[113], Y. Ding[126,6], R. Divià[32], D. U. Dixit[18],
Ø.. Djuvsland[20], U. Dmitrieva[140], A. Dobrin[62], B. Dönigus[63], A. K. Dubey[132], J. M. Dubinski[133], A. Dubla[98],
S. Dudi[90], P. Dupieux[125], M. Durkac[106], N. Dzalaiova[12], T. M. Eder[135], R. J. Ehlers[87], V. N. Eikeland[20],
F. Eisenhut[63], D. Elia[49], B. Erazmus[104], F. Ercolessi[25], F. Erhardt[89], M. R. Ersdal[20], B. Espagnon[72],
G. Eulisse[32], D. Evans[101], S. Evdokimov[140], L. Fabbietti[96], M. Faggin[27], J. Faivre[73], F. Fan[6],
W. Fan[74], A. Fantoni[48], M. Fasel[87], P. Fecchio[29], A. Feliciello[55], G. Feofilov[140], A. Fernández Téllez[44],
M. B. Ferrer[32], A. Ferrero[128], A. Ferretti[24], V. J. G. Feuillard[95], J. Figiel[107], V. Filova[35], D. Finogeev[140],
F. M. Fionda[51], G. Fiorenza[97], F. Flor[114], A. N. Flores[108], S. Foertsch[67], I. Fokin[95], S. Fokin[140],
E. Fragiacomo[56], E. Frajna[136], U. Fuchs[32], N. Funicello[28], C. Furget[73], A. Furs[140], T. Fusayasu[99],
J. J. Gaardhøje[83], M. Gagliardi[24], A. M. Gago[102], A. Gal[127], C. D. Galvan[109], D. R. Gangadharan[114],
P. Ganoti[78], C. Garabatos[98], J. R. A. Garcia[44], E. Garcia-Solis[9], K. Garg[104], C. Gargiulo[32], A. Garibli[81],
K. Garner[135], A. Gautam[116], M. B. Gay Ducati[65], M. Germain[104], C. Ghosh[132], S. K. Ghosh[4], M. Giacalone[25],
P. Gianotti[48], P. Giubellino[98,55], P. Giubilato[27], A. M. C. Glaenzer[128], P. Glässel[95], E. Glimos[120],
D. J. Q. Goh[76], V. Gonzalez[134], L. H. González-Trueba[66], S. Gorbunov[38], M. Gorgon[2], L. Görlich[107],
S. Gotovac[33], V. Grabski[66], L. K. Graczykowski[133], E. Grecka[86], L. Greiner[74], A. Grelli[58], C. Grigoras[32],
V. Grigoriev[140], S. Grigoryan[141,1], F. Grosa[32], J. F. Grosse-Oetringhaus[32], R. Grosso[98], D. Grund[35],
G. G. Guardiano[111], R. Guernane[73], M. Guilbaud[104], K. Gulbrandsen[83], T. Gunji[122], W. Guo[6], A. Gupta[91],
R. Gupta[91], S. P. Guzman[44], L. Gyulai[136], M. K. Habib[98], C. Hadjidakis[72], H. Hamagaki[76], M. Hamid[6],
Y. Han[138], R. Hannigan[108], M. R. Haque[133], A. Harlenderova[98], J. W. Harris[137], A. Harton[9], H. Hassan[87],
D. Hatzifotiadou[50], P. Hauer[42], L. B. Havener[137], S. T. Heckel[96], E. Hellbär[98], H. Helstrup[34], T. Herman[35],
G. Herrera Corral[8], F. Herrmann[135], S. Herrmann[126], K. F. Hetland[34], B. Heybeck[63], H. Hillemanns[32],
C. Hills[117], B. Hippolyte[127], B. Hofman[58], B. Hohlweger[84], J. Honermann[135], G. H. Hong[138], D. Horak[35],
A. Horzyk[2], R. Hosokawa[14], Y. Hou[6], P. Hristov[32], C. Hughes[120], P. Huhn[63], L. M. Huhta[115], C. V. Hulse[72],
T. J. Humanic[88], H. Hushnud[100], L. A. Husova[135], A. Hutson[114], J. P. Iddon[117], R. Ilkaev[140], H. Ilyas[13],
M. Inaba[123], G. M. Innocenti[32], M. Ippolitov[140], A. Isakov[86], T. Isidori[116], M. S. Islam[100], M. Ivanov[12],
M. Ivanov[98], V. Ivanov[140], V. Izucheev[140], M. Jablonski[2], B. Jacak[74], N. Jacazio[32], P. M. Jacobs[74],
S. Jadlovska[106], J. Jadlovsky[106], S. Jaelani[82], L. Jaffe[38], C. Jahnke[111], M. A. Janik[133], T. Janson[69], M. Jercic[89],
O. Jevons[101], A. A. P. Jimenez[64], F. Jonas[87], P. G. Jones[101], J. M. Jowett[32,98], J. Jung[63], M. Jung[63],
A. Junique[32], A. Jusko[101], M. J. Kabus[32,133], J. Kaewjai[105], P. Kalinak[59], A. S. Kalteyer[98], A. Kalweit[32],
V. Kaplin[140], A. Karasu Uysal[71], D. Karatovic[89], O. Karavichev[140], T. Karavicheva[140], P. Karczmarczyk[133],
E. Karpechev[140], V. Kashyap[80], A. Kazantsev[140], U. Kebschull[69], R. Keidel[139], D. L. D. Keijdener[58], M. Keil[32],
B. Ketzer[42], A. M. Khan[6], S. Khan[15], A. Khanzadeev[140], Y. Kharlov[140], A. Khatun[15], A. Khuntia[107],
B. Kileng[34], B. Kim[16], C. Kim[16], D. J. Kim[115], E. J. Kim[68], J. Kim[138], J. S. Kim[40], J. Kim[95], J. Kim[68],
M. Kim[95], S. Kim[17], T. Kim[138], K. Kimura[93], S. Kirsch[63], I. Kisel[38], S. Kiselev[140], A. Kisiel[133],
J. P. Kitowski[2], J. L. Klay[5], J. Klein[32], S. Klein[74], C. Klein-Bösing[135], M. Kleiner[63], T. Klemenz[96],
A.. Kluge[32], A. G. Knospe[114], C. Kobdaj[105], T. Kollegger[98], A. Kondratyev[141], E. Kondratyuk[140], J. Konig[63],
S. A. Konigstorfer[96], P. J. Konopka[32], G. Kornakov[133], S. D. Koryciak[2], A. Kotliarov[86], O. Kovalenko[79],
V. Kovalenko[140], M. Kowalski[107], I. Králik[59], A. Kravčáková[37], L. Kreis[98], M. Krivda[101,59], F. Krizek[86],
K. Krizkova Gajdosova[35], M. Kroesen[95], M. Krüger[63], D. M. Krupova[35], E. Kryshen[140], M. Krzewicki[38],
V. Kučera[32], C. Kuhn[127], P. G. Kuijer[84], T. Kumaoka[123], D. Kumar[132], L. Kumar[90], N. Kumar[90], S. Kundu[32],
P. Kurashvili[79], A. Kurepin[140], A. B. Kurepin[140], S. Kushpil[86], J. Kvapil[101], M. J. Kweon[57], J. Y. Kwon[57],
Y. Kwon[138], S. L. La Pointe[38], P. La Rocca[26], Y. S. Lai[74], A. Lakrathok[105], M. Lamanna[32], R. Langoy[119],
P. Larionov[48], E. Laudi[32], L. Lautner[32,96], R. Lavicka[103], T. Lazareva[140], R. Lea[131,54], G. Legras[135],

J. Lehrbach[38], R. C. Lemmon[85], I. León Monzón[109], M. M. Lesch[96], E. D. Lesser[18], M. Lettrich[96], P. Lévai[136], X. Li[10], X. L. Li[6], J. Lien[119], R. Lietava[101], B. Lim[16], S. H. Lim[16], V. Lindenstruth[38], A. Lindner[45], C. Lippmann[98], A. Liu[18], D. H. Liu[6], J. Liu[117], I. M. Lofnes[20], C. Loizides[87], P. Loncar[33], J. A. Lopez[95], X. Lopez[125], E. López Torres[7], P. Lu[98,118], J. R. Luhder[135], M. Lunardon[27], G. Luparello[56], Y. G. Ma[39], A. Maevskaya[140], M. Mager[32], T. Mahmoud[42], A. Maire[127], M. Malaev[140], G. Malfattore[25], N. M. Malik[91], Q. W. Malik[19], S. K. Malik[91], L. Malinina[141,f], D. Mal'Kevich[140], D. Mallick[80], N. Mallick[47], G. Mandaglio[30,52], V. Manko[140], F. Manso[125], V. Manzari[49], Y. Mao[6], G. V. Margagliotti[23], A. Margotti[50], A. Marín[98], C. Markert[108], M. Marquard[63], P. Martinengo[32], J. L. Martinez[114], M. I. Martínez[44], G. Martínez García[104], S. Masciocchi[98], M. Masera[24], A. Masoni[51], L. Massacrier[72], A. Mastroserio[129,49], A. M. Mathis[96], O. Matonoha[75], P. F. T. Matuoka[110], A. Matyja[107], C. Mayer[107], A. L. Mazuecos[32], F. Mazzaschi[24], M. Mazzilli[32], J. E. Mdhluli[121], A. F. Mechler[63], Y. Melikyan[140], A. Menchaca-Rocha[66], E. Meninno[103,28], A. S. Menon[114], M. Meres[12], S. Mhlanga[113,67], Y. Miake[123], L. Micheletti[55], L. C. Migliorin[126], D. L. Mihaylov[96], K. Mikhaylov[141,140], A. N. Mishra[136], D. Miśkowiec[98], A. Modak[4], A. P. Mohanty[58], B. Mohanty[80], M. Mohisin Khan[15,c], M. A. Molander[43], Z. Moravcova[83], C. Mordasini[96], D. A. Moreira De Godoy[135], I. Morozov[140], A. Morsch[32], T. Mrnjavac[32], V. Muccifora[48], E. Mudnic[33], S. Muhuri[132], J. D. Mulligan[74], A. Mulliri[22], M. G. Munhoz[110], R. H. Munzer[63], H. Murakami[122], S. Murray[113], L. Musa[32], J. Musinsky[59], J. W. Myrcha[133], B. Naik[121], R. Nair[79], A. I. Nambrath[18], B. K. Nandi[46], R. Nania[50], E. Nappi[49], A. F. Nassirpour[75], A. Nath[95], C. Nattrass[120], A. Neagu[19], A. Negru[124], L. Nellen[64], S. V. Nesbo[34], G. Neskovic[38], D. Nesterov[140], B. S. Nielsen[83], E. G. Nielsen[83], S. Nikolaev[140], S. Nikulin[140], V. Nikulin[140], F. Noferini[50], S. Noh[11], P. Nomokonov[141], J. Norman[117], N. Novitzky[123], P. Nowakowski[133], A. Nyanin[140], J. Nystrand[20], M. Ogino[76], A. Ohlson[75], V. A. Okorokov[140], J. Oleniacz[133], A. C. Oliveira Da Silva[120], M. H. Oliver[137], A. Onnerstad[115], C. Oppedisano[55], A. Ortiz Velasquez[64], A. Oskarsson[75], J. Otwinowski[107], M. Oya[93], K. Oyama[76], Y. Pachmayer[95], S. Padhan[46], D. Pagano[131,54], G. Paić[64], A. Palasciano[49], S. Panebianco[128], H. Park[123], J. Park[57], J. E. Parkkila[32,115], S. P. Pathak[114], R. N. Patra[91], B. Paul[22], H. Pei[6], T. Peitzmann[58], X. Peng[6], M. Pennisi[24], L. G. Pereira[65], H. Pereira Da Costa[128], D. Peresunko[140], G. M. Perez[7], S. Perrin[128], Y. Pestov[140], V. Petráček[35], V. Petrov[140], M. Petrovici[45], R. P. Pezzi[104,65], S. Piano[56], M. Pikna[12], P. Pillot[104], O. Pinazza[50,32], L. Pinsky[114], C. Pinto[96], S. Pisano[48], M. Płoskoń[74], M. Planinic[89], F. Pliquett[63], M. G. Poghosyan[87], S. Politano[29], N. Poljak[89], A. Pop[45], S. Porteboeuf-Houssais[125], J. Porter[74], V. Pozdniakov[141], S. K. Prasad[4], S. Prasad[47], R. Preghenella[50], F. Prino[55], C. A. Pruneau[134], I. Pshenichnov[140], M. Puccio[32], S. Pucillo[24], Z. Pugelova[106], S. Qiu[84], L. Quaglia[24], R. E. Quishpe[114], S. Ragoni[101], A. Rakotozafindrabe[128], L. Ramello[130,55], F. Rami[127], S. A. R. Ramirez[44], T. A. Rancien[73], R. Raniwala[92], S. Raniwala[92], S. S. Räsänen[43], R. Rath[50,47], I. Ravasenga[84], K. F. Read[87,120], A. R. Redelbach[38], K. Redlich[79,d], A. Rehman[20], P. Reichelt[63], F. Reidt[32], H. A. Reme-Ness[34], Z. Rescakova[37], K. Reygers[95], A. Riabov[140], V. Riabov[140], R. Ricci[28], T. Richert[75], M. Richter[19], A. A. Riedel[96], W. Riegler[32], F. Riggi[26], C. Ristea[62], M. Rodríguez Cahuantzi[44], K. Røed[19], R. Rogalev[140], E. Rogochaya[141], T. S. Rogoschinski[63], D. Rohr[32], D. Röhrich[20], P. F. Rojas[44], S. Rojas Torres[35], P. S. Rokita[133], G. Romanenko[141], F. Ronchetti[48], A. Rosano[30,52], E. D. Rosas[64], A. Rossi[53], A. Roy[47], P. Roy[100], S. Roy[46], N. Rubini[25], O. V. Rueda[75], D. Ruggiano[133], R. Rui[23], B. Rumyantsev[141], P. G. Russek[2], R. Russo[84], A. Rustamov[81], E. Ryabinkin[140], Y. Ryabov[140], A. Rybicki[107], H. Rytkonen[115], W. Rzesa[133], O. A. M. Saarimaki[43], R. Sadek[104], S. Sadovsky[140], J. Saetre[20], K. Šafařík[35], S. Saha[80], B. Sahoo[46], R. Sahoo[47], S. Sahoo[60], D. Sahu[47], P. K. Sahu[60], J. Saini[132], K. Sajdakova[37], S. Sakai[123], M. P. Salvan[98], S. Sambyal[91], T. B. Saramela[110], D. Sarkar[134], N. Sarkar[132], P. Sarma[41], V. Sarritzu[22], V. M. Sarti[96], M. H. P. Sas[137], J. Schambach[87], H. S. Scheid[63], C. Schiaua[45], R. Schicker[95], A. Schmah[95], C. Schmidt[98], H. R. Schmidt[94], M. O. Schmidt[32], M. Schmidt[94], N. V. Schmidt[87], A. R. Schmier[120], R. Schotter[127], J. Schukraft[32], K. Schwarz[98], K. Schweda[98], G. Scioli[25], E. Scomparin[55], J. E. Seger[14], Y. Sekiguchi[122], D. Sekihata[122], I. Selyuzhenkov[98,140], S. Senyukov[127], J. J. Seo[57], D. Serebryakov[140], L. Šerkšnytė[96], A. Sevcenco[62], T. J. Shaba[67], A. Shabetai[104], R. Shahoyan[32], A. Shangaraev[140], A. Sharma[90], D. Sharma[46], H. Sharma[107], M. Sharma[91], N. Sharma[90], S. Sharma[76], S. Sharma[91], U. Sharma[91], A. Shatat[72], O. Sheibani[114], K. Shigaki[93], M. Shimomura[77], S. Shirinkin[140], Q. Shou[39], Y. Sibiriak[140], S. Siddhanta[51], T. Siemiarczuk[79], T. F. Silva[110], D. Silvermyr[75], T. Simantathammakul[105], R. Simeonov[36], G. Simonetti[32], B. Singh[91], B. Singh[96], R. Singh[80], R. Singh[91], R. Singh[47], S. Singh[15], V. K. Singh[132], V. Singhal[132], T. Sinha[100], B. Sitar[12], M. Sitta[130,55], T. B. Skaali[19], G. Skorodumovs[95], M. Slupecki[43], N. Smirnov[137], R. J. M. Snellings[58], E. H. Solheim[19], C. Soncco[102], J. Song[114], A. Songmoolnak[105],

F. Soramel[27], S. Sorensen[120], R. Spijkers[84], I. Sputowska[107], J. Staa[75], J. Stachel[95], I. Stan[62], P. J. Steffanic[120], S. F. Stiefelmaier[95], D. Stocco[104], I. Storehaug[19], M. M. Storetvedt[34], P. Stratmann[135], S. Strazzi[25], C. P. Stylianidis[84], A. A. P. Suaide[110], C. Suire[72], M. Sukhanov[140], M. Suljic[32], V. Sumberia[91], S. Sumowidagdo[82], S. Swain[60], I. Szarka[12], U. Tabassam[13], S. F. Taghavi[96], G. Taillepied[98], J. Takahashi[111], G. J. Tambave[20], S. Tang[125,6], Z. Tang[118], J. D. Tapia Takaki[116,e], N. Tapus[124], M. G. Tarzila[45], G. F. Tassielli[31], A. Tauro[32], A. Telesca[32], L. Terlizzi[24], C. Terrevoli[114], G. Tersimonov[3], D. Thomas[108], A. Tikhonov[140], A. R. Timmins[114], M. Tkacik[106], T. Tkacik[106], A. Toia[63], R. Tokumoto[93], N. Topilskaya[140], M. Toppi[48], F. Torales-Acosta[18], T. Tork[72], A. G. Torres Ramos[31], A. Trifiró[30,52], A. S. Triolo[30,52], S. Tripathy[50], T. Tripathy[46], S. Trogolo[32], V. Trubnikov[3], W. H. Trzaska[115], T. P. Trzcinski[133], R. Turrisi[53], T. S. Tveter[19], K. Ullaland[20], B. Ulukutlu[96], A. Uras[126], M. Urioni[54,131], G. L. Usai[22], M. Vala[37], N. Valle[21], S. Vallero[55], L. V. R. van Doremalen[58], M. van Leeuwen[84], C. A. van Veen[95], R. J. G. van Weelden[84], P. Vande Vyvre[32], D. Varga[136], Z. Varga[136], M. Varga-Kofarago[136], M. Vasileiou[78], A. Vasiliev[140], O. Vázquez Doce[96], V. Vechernin[140], E. Vercellin[24], S. Vergara Limón[44], L. Vermunt[98], R. Vértesi[136], M. Verweij[58], L. Vickovic[33], Z. Vilakazi[121], O. Villalobos Baillie[101], G. Vino[49], A. Vinogradov[140], T. Virgili[28], V. Vislavicius[83], A. Vodopyanov[141], B. Volkel[32], M. A. Völkl[95], K. Voloshin[140], S. A. Voloshin[134], G. Volpe[31], B. von Haller[32], I. Vorobyev[96], N. Vozniuk[140], J. Vrláková[37], B. Wagner[20], C. Wang[39], D. Wang[39], M. Weber[103], A. Wegrzynek[32], F. T. Weiglhofer[38], S. C. Wenzel[32], J. P. Wessels[135], S. L. Weyhmiller[137], J. Wiechula[63], J. Wikne[19], G. Wilk[79], J. Wilkinson[98], G. A. Willems[135], B. Windelband[95], M. Winn[128], J. R. Wright[108], W. Wu[39], Y. Wu[118], R. Xu[6], A. Yadav[42], A. K. Yadav[132], S. Yalcin[71], Y. Yamaguchi[93], K. Yamakawa[93], S. Yang[20], S. Yano[93], Z. Yin[6], I.-K. Yoo[16], J. H. Yoon[57], S. Yuan[20], A. Yuncu[95], V. Zaccolo[23], C. Zampolli[32], H. J. C. Zanoli[58], F. Zanone[95], N. Zardoshti[32,101], A. Zarochentsev[140], P. Závada[61], N. Zaviyalov[140], M. Zhalov[140], B. Zhang[6], S. Zhang[39], X. Zhang[6], Y. Zhang[118], Z. Zhang[6], M. Zhao[10], V. Zherebchevskii[140], Y. Zhi[10], N. Zhigareva[140], D. Zhou[6], Y. Zhou[83], J. Zhu[98,6], Y. Zhu[6], G. Zinovjev[3,*], N. Zurlo[131,54]

[1] A.I. Alikhanyan National Science Laboratory (Yerevan Physics Institute) Foundation, Yerevan, Armenia

[2] AGH University of Science and Technology, Cracow, Poland

[3] Bogolyubov Institute for Theoretical Physics, National Academy of Sciences of Ukraine, Kiev, Ukraine

[4] Bose Institute, Department of Physics and Centre for Astroparticle Physics and Space Science (CAPSS), Kolkata, India

[5] California Polytechnic State University, San Luis Obispo, CA, USA

[6] Central China Normal University, Wuhan, China

[7] Centro de Aplicaciones Tecnológicas y Desarrollo Nuclear (CEADEN), Havana, Cuba

[8] Centro de Investigación y de Estudios Avanzados (CINVESTAV), Mexico City and Mérida, Mexico

[9] Chicago State University, Chicago, IL, USA

[10] China Institute of Atomic Energy, Beijing, China

[11] Chungbuk National University, Cheongju, Republic of Korea

[12] Comenius University Bratislava, Faculty of Mathematics, Physics and Informatics, Bratislava, Slovak Republic

[13] COMSATS University Islamabad, Islamabad, Pakistan

[14] Creighton University, Omaha, NE, USA

[15] Department of Physics, Aligarh Muslim University, Aligarh, India

[16] Department of Physics, Pusan National University, Pusan, Republic of Korea

[17] Department of Physics, Sejong University, Seoul, Republic of Korea

[18] Department of Physics, University of California, Berkeley, CA, USA

[19] Department of Physics, University of Oslo, Oslo, Norway

[20] Department of Physics and Technology, University of Bergen, Bergen, Norway

[21] Dipartimento di Fisica, Università di Pavia, Pavia, Italy

[22] Dipartimento di Fisica dell'Università and Sezione INFN, Cagliari, Italy

[23] Dipartimento di Fisica dell'Università and Sezione INFN, Trieste, Italy

[24] Dipartimento di Fisica dell'Università and Sezione INFN, Turin, Italy

[25] Dipartimento di Fisica e Astronomia dell'Università and Sezione INFN, Bologna, Italy

[26] Dipartimento di Fisica e Astronomia dell'Università and Sezione INFN, Catania, Italy

[27] Dipartimento di Fisica e Astronomia dell'Università and Sezione INFN, Padua, Italy

[28] Dipartimento di Fisica 'E.R. Caianiello' dell'Università and Gruppo Collegato INFN, Salerno, Italy

[29] Dipartimento DISAT del Politecnico and Sezione INFN, Turin, Italy

[30] Dipartimento di Scienze MIFT, Università di Messina, Messina, Italy

[31] Dipartimento Interateneo di Fisica 'M. Merlin' and Sezione INFN, Bari, Italy

[32] European Organization for Nuclear Research (CERN), Geneva, Switzerland

[33] Faculty of Electrical Engineering, Mechanical Engineering and Naval Architecture, University of Split, Split, Croatia

[34] Faculty of Engineering and Science, Western Norway University of Applied Sciences, Bergen, Norway

[35] Faculty of Nuclear Sciences and Physical Engineering, Czech Technical University in Prague, Prague, Czech Republic

[36] Faculty of Physics, Sofia University, Sofia, Bulgaria

[37] Faculty of Science, P.J. Šafárik University, Košice, Slovak Republic

[38] Frankfurt Institute for Advanced Studies, Johann Wolfgang Goethe-Universität Frankfurt, Frankfurt, Germany

[39] Fudan University, Shanghai, China

[40] Gangneung-Wonju National University, Gangneung, Republic of Korea

[41] Gauhati University, Department of Physics, Guwahati, India

[42] Helmholtz-Institut für Strahlen- und Kernphysik, Rheinische Friedrich-Wilhelms-Universität Bonn, Bonn, Germany

[43] Helsinki Institute of Physics (HIP), Helsinki, Finland

[44] High Energy Physics Group, Universidad Autónoma de Puebla, Puebla, Mexico

[45] Horia Hulubei National Institute of Physics and Nuclear Engineering, Bucharest, Romania

[46] Indian Institute of Technology Bombay (IIT), Mumbai, India

[47] Indian Institute of Technology Indore, Indore, India

[48] INFN, Laboratori Nazionali di Frascati, Frascati, Italy

[49] INFN, Sezione di Bari, Bari, Italy

[50] INFN, Sezione di Bologna, Bologna, Italy

[51] INFN, Sezione di Cagliari, Cagliari, Italy

[52] INFN, Sezione di Catania, Catania, Italy

[53] INFN, Sezione di Padova, Padua, Italy

[54] INFN, Sezione di Pavia, Pavia, Italy

[55] INFN, Sezione di Torino, Turin, Italy

[56] INFN, Sezione di Trieste, Trieste, Italy

[57] Inha University, Incheon, Republic of Korea

[58] Institute for Gravitational and Subatomic Physics (GRASP), Utrecht University/Nikhef, Utrecht, The Netherlands

[59] Institute of Experimental Physics, Slovak Academy of Sciences, Košice, Slovak Republic

[60] Institute of Physics, Homi Bhabha National Institute, Bhubaneswar, India

[61] Institute of Physics of the Czech Academy of Sciences, Prague, Czech Republic

[62] Institute of Space Science (ISS), Bucharest, Romania

[63] Institut für Kernphysik, Johann Wolfgang Goethe-Universität Frankfurt, Frankfurt, Germany

[64] Instituto de Ciencias Nucleares, Universidad Nacional Autónoma de México, Mexico City, Mexico

[65] Instituto de Física, Universidade Federal do Rio Grande do Sul (UFRGS), Porto Alegre, Brazil

[66] Instituto de Física, Universidad Nacional Autónoma de México, Mexico City, Mexico

[67] iThemba LABS, National Research Foundation, Somerset West, South Africa

[68] Jeonbuk National University, Jeonju, Republic of Korea

[69] Johann-Wolfgang-Goethe Universität Frankfurt Institut für Informatik, Fachbereich Informatik und Mathematik, Frankfurt, Germany

[70] Korea Institute of Science and Technology Information, Daejeon, Republic of Korea

[71] KTO Karatay University, Konya, Turkey

[72] Laboratoire de Physique des 2 Infinis, Irène Joliot-Curie, Orsay, France

[73] Laboratoire de Physique Subatomique et de Cosmologie, Université Grenoble-Alpes, CNRS-IN2P3, Grenoble, France

[74] Lawrence Berkeley National Laboratory, Berkeley, California, USA

[75] Lund University Department of Physics, Division of Particle Physics, Lund, Sweden

[76] Nagasaki Institute of Applied Science, Nagasaki, Japan

[77] Nara Women's University (NWU), Nara, Japan

[78] National and Kapodistrian University of Athens, School of Science, Department of Physics , Athens, Greece

[79] National Centre for Nuclear Research, Warsaw, Poland

[80] National Institute of Science Education and Research, Homi Bhabha National Institute, Jatni, India

[81] National Nuclear Research Center, Baku, Azerbaijan

[82] National Research and Innovation Agency - BRIN, Jakarta, Indonesia

[83] Niels Bohr Institute, University of Copenhagen, Copenhagen, Denmark

[84] Nikhef, National institute for subatomic physics, Amsterdam, The Netherlands

[85] Nuclear Physics Group, STFC Daresbury Laboratory, Daresbury, UK

[86] Nuclear Physics Institute of the Czech Academy of Sciences, Husinec-Řež, Czech Republic

[87] Oak Ridge National Laboratory, Oak Ridge, TN, USA

[88] Ohio State University, Columbus, OH, USA

[89] Physics department, Faculty of science, University of Zagreb, Zagreb, Croatia

[90] Physics Department, Panjab University, Chandigarh, India

[91] Physics Department, University of Jammu, Jammu, India

[92] Physics Department, University of Rajasthan, Jaipur, India

[93] Physics Program and International Institute for Sustainability with Knotted Chiral Meta Matter (SKCM2), Hiroshima University, Hiroshima, Japan

[94] Physikalisches Institut, Eberhard-Karls-Universität Tübingen, Tübingen, Germany

[95] Physikalisches Institut, Ruprecht-Karls-Universität Heidelberg, Heidelberg, Germany

[96] Physik Department, Technische Universität München, Munich, Germany

[97] Politecnico di Bari and Sezione INFN, Bari, Italy

[98] Research Division and ExtreMe Matter Institute EMMI, GSI Helmholtzzentrum für Schwerionenforschung GmbH, Darmstadt, Germany

[99] Saga University, Saga, Japan

[100] Saha Institute of Nuclear Physics, Homi Bhabha National Institute, Kolkata, India

[101] School of Physics and Astronomy, University of Birmingham, Birmingham, United Kingdom

[102] Sección Física, Departamento de Ciencias, Pontificia Universidad Católica del Perú, Lima, Peru

[103] Stefan Meyer Institut für Subatomare Physik (SMI), Vienna, Austria

[104] SUBATECH, IMT Atlantique, Nantes Université, CNRS-IN2P3, Nantes, France

[105] Suranaree University of Technology, Nakhon Ratchasima, Thailand

[106] Technical University of Košice, Košice, Slovak Republic

[107] The Henryk Niewodniczanski Institute of Nuclear Physics, Polish Academy of Sciences, Cracow, Poland

[108] The University of Texas at Austin, Austin, TX, USA

[109] Universidad Autónoma de Sinaloa, Culiacán, Mexico

[110] Universidade de São Paulo (USP), São Paulo, Brazil

[111] Universidade Estadual de Campinas (UNICAMP), Campinas, Brazil

[112] Universidade Federal do ABC, Santo Andre, Brazil

[113] University of Cape Town, Cape Town, South Africa

[114] University of Houston, Houston, TX, USA

[115] University of Jyväskylä, Jyväskylä, Finland

[116] University of Kansas, Lawrence, KS, USA

[117] University of Liverpool, Liverpool, UK

[118] University of Science and Technology of China, Hefei, China

[119] University of South-Eastern Norway, Kongsberg, Norway

[120] University of Tennessee, Knoxville, TN, USA

[121] University of the Witwatersrand, Johannesburg, South Africa

[122] University of Tokyo, Tokyo, Japan

[123] University of Tsukuba, Tsukuba, Japan

[124] University Politehnica of Bucharest, Bucharest, Romania

[125] Université Clermont Auvergne, CNRS/IN2P3, LPC, Clermont-Ferrand, France

[126] Université de Lyon, CNRS/IN2P3, Institut de Physique des 2 Infinis de Lyon, Lyon, France

[127] Université de Strasbourg, CNRS, IPHC UMR 7178, F-67000 Strasbourg, France, Strasbourg, France

[128] Départment de Physique Nucléaire (DPhN), Université Paris-Saclay Centre d'Etudes de Saclay (CEA), IRFU, Saclay, France

[129] Università degli Studi di Foggia, Foggia, Italy

[130] Università del Piemonte Orientale, Vercelli, Italy

[131] Università di Brescia, Brescia, Italy

[132] Variable Energy Cyclotron Centre, Homi Bhabha National Institute, Kolkata, India

[133] Warsaw University of Technology, Warsaw, Poland

[134] Wayne State University, Detroit, MI, USA

[135] Westfälische Wilhelms-Universität Münster, Institut für Kernphysik, Münster, Germany

[136] Wigner Research Centre for Physics, Budapest, Hungary

[137] Yale University, New Haven, CT, USA

[138] Yonsei University, Seoul, Republic of Korea

[139] Zentrum für Technologie und Transfer (ZTT), Worms, Germany

[140] Affiliated with an Institute Covered by a Cooperation Agreement with CERN, Geneva, Switzerland

[141] Affiliated with an International Laboratory Covered by a Cooperation Agreement with CERN, Geneva 23, Switzerland

[a] Also at: Italian National Agency for New Technologies, Energy and Sustainable Economic Development (ENEA), Bologna, Italy

[b] Also at: Dipartimento DET del Politecnico di Torino, Turin, Italy

[c] Also at: Department of Applied Physics, Aligarh Muslim University, Aligarh, India

[d] Also at: Institute of Theoretical Physics, University of Wroclaw, Poland

[e] Also at: University of Kansas, Lawrence, KS, USA

[f] Also at: An Institution Covered by a Cooperation Agreement with CERN, Geneva, Switzerland

* Deceased